# Damage Development in Cementitious Materials Exposed to Magnesium Chloride Deicing Salt

Yaghoob Farnam[(1)], Andrew Wiese[(2)], Dale Bentz[(3)], Jeffrey Davis[(4)], Jason Weiss[(5)]

[(1)] Graduate Research Assistant, Lyles School of Civil Engineering, Purdue University, 550 Stadium Mall Dr., West Lafayette, IN 47907, USA, yfarnam@purdue.edu

[(2)] Graduate Research Assistant, Lyles School of Civil Engineering, Purdue University, 550 Stadium Mall Dr., West Lafayette, IN 47907, USA, awiese@purdue.edu

[(3)] Chemical Engineer, Materials and Structural Systems Division, National Institute of Standards and Technology, 100 Bureau Drive, Stop 8615, Gaithersburg, MD 20899, USA, dale.bentz@nist.gov

[(4)] Materials Research Engineer, Materials Measurement Science Division, National Institute of Standards and Technology, 100 Bureau Drive, Gaithersburg, MD 20899, USA, jeff.davis@nist.gov

[(5)] Jack and Kay Hockema Professor of Civil Engineering, Director of Pankow Materials Laboratory, Lyles School of Civil Engineering, Purdue University, 550 Stadium Mall Dr., West Lafayette, IN 47907, wjweiss@purdue.edu

24    ABSTRACT

25        Magnesium chloride ($MgCl_2$) is used in deicing applications due to its capability to

26    depress freezing temperatures to a lower point than other salts such as sodium chloride (NaCl).

27    The constituents of concrete (i.e., pores solution, calcium hydroxide, aluminate phases, and

28    calcium silicate hydrate gel) can alter the $MgCl_2$–$H_2O$ phase diagram when it is used to interpret

29    the performance of concrete. Different chemical reactions may concurrently occur between

30    $MgCl_2$ and cementitious constituents to form Brucite, Friedel's salts, magnesium silicate hydrate,

31    magnesium oxychloride, and/or secondary calcium oxychloride. In this study, it was observed

32    that $MgCl_2$ can be entirely consumed in concrete by the chemical reactions and produce $CaCl_2$.

33    As such, it was found that $MgCl_2$ interacts significantly with a cementitious material and it follows

34    a response that is more similar to the $Ca(OH)_2$-$CaCl_2$-$H_2O$ phase diagram than that of the

35    $MgCl_2$–$H_2O$ phase diagram. Mortar samples exposed to low concentration $MgCl_2$ solutions (<10

36    % by mass) for a short duration of freezing and thawing showed damage due to ice formation,

37    while for higher concentrations (≥10 % by mass), the damage was most likely due to the

38    chemical reactions between $MgCl_2$ and cementitious constituents at room temperature (23 °C).

39    These chemical reactions occurred rapidly (within 5-10 min) and caused a significant decrease

40    in subsequent fluid ingress into exposed concrete.

41

42    Keywords: Brucite, Concrete, Deicing Salt, Freeze-Thaw, Damage, Magnesium Oxychloride,

43    Magnesium Silicate Hydrate (M-S-H), Phase Change, Calcium Oxychloride.

44

## 1.0 Introduction

The widespread use of deicing salt is considered to be a primary cause of the deterioration of concrete structures in cold climates, resulting in costly repairs and early replacement of concrete infrastructure elements. Deicing salts can penetrate into the concrete and cause corrosion of reinforcement, as well as changing the concrete microstructure by participating in aggressive chemical reactions. Changes in concrete microstructure due to aggressive chemical reactions are often accompanied by a decrease in the mechanical properties, a change in transport resistance of concrete, and damage and degradation. The formation of expansive phases and salt crystallization in concrete pores are thus two major sources of damage and cracking in a concrete exposed to deicing salts [1–7].

Among the most common deicing chemicals, $MgCl_2$ is perceived as being particularly effective in melting ice and snow due to: 1) its ability to depress the freezing temperature of a solution to a lower temperature than other salts (Figure 1) and 2) dissolution of $MgCl_2$ itself can produce heat that can be further used to melt ice or snow (enthalpy of hydration = -2653 kJ/mol). However, concrete exposed to $MgCl_2$ de-icing salt typically exhibits changes in its microstructure due to chemical reactions, including formation of brucite, Friedel's salts, magnesium silicate hydrate (M-S-H), magnesium oxychloride, and/or secondary calcium oxychloride; these changes can be accompanied by severe cracking, even if the concrete does not experience any freezing and thawing cycles [5,8–10].
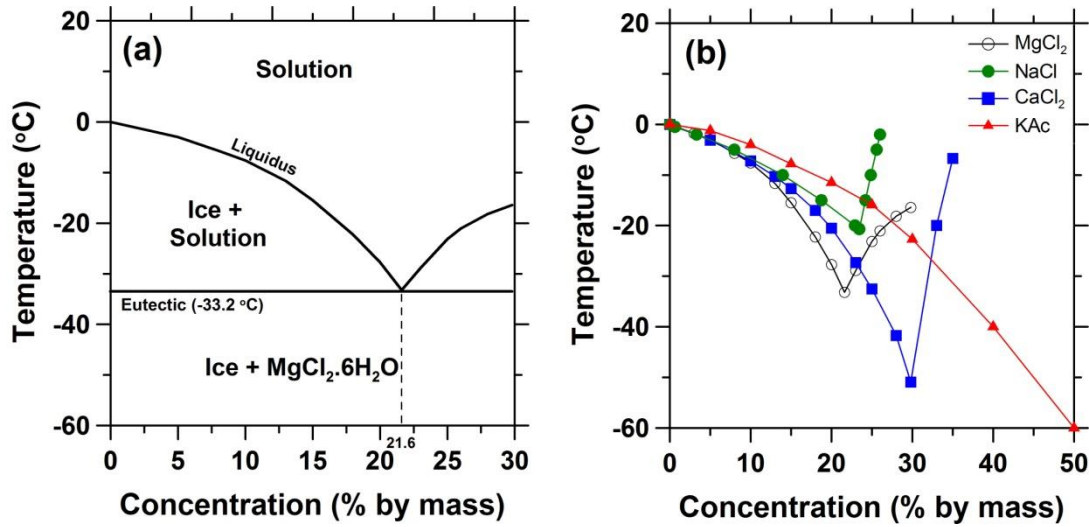
*Figure 1 – a) Phase diagram for $MgCl_2$-$H_2O$ and b) comparison of freezing temperature for aqueous $MgCl_2$ with NaCl, $CaCl_2$, and KAc (potassium acetate) deicing chemicals.*
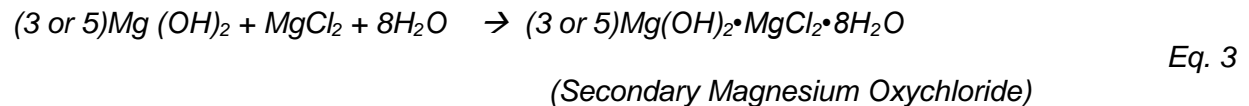
$MgCl_2$ deicers can react with the cement paste to produce M-S-H and brucite ($Mg(OH)_2$). As described in Eq. 1, non cementitious magnesium silicate hydrate is formed by replacing the calcium from the cementitious calcium silicate hydrate (C-S-H) with magnesium. The formation of M-S-H was reported to produce damage in concrete and it appears to be a gradual and slow reacting product [8,11].
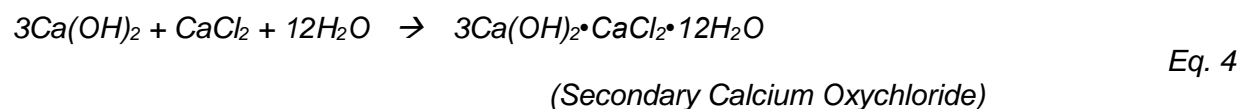
$$C\text{-}S\text{-}H + MgCl_2 \rightarrow CaCl_2 + M\text{-}S\text{-}H \qquad\qquad (M\text{-}S\text{-}H) \qquad\qquad Eq.\ 1$$

The formation of brucite is caused by $MgCl_2$ reacting with $Ca(OH)_2$ as shown in Eq. 2. In the presence of reactive dolomite aggregate, brucite formation resulted in mechanical distress [12]. The brucite usually forms on the surface of concrete samples as an outer layer product [5,8,13–15]. The brucite appears to be a dense and homogeneous product [15]. It is also reported that the brucite layer can slow down concrete deterioration due to deicing salt exposure by hindering ingress of the chloride solution into the concrete [8].
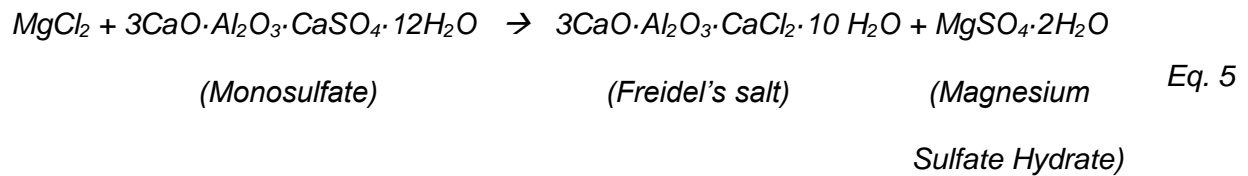
$$Ca(OH)_2 + MgCl_2 \rightarrow CaCl_2 + Mg(OH)_2 \qquad\qquad (Brucite) \qquad\qquad Eq.\ 2$$

3

80      Formations of magnesium oxychloride and calcium oxychloride were also reported in

81    concrete with $MgCl_2$ as secondary reactions [5,7,10], since $CaCl_2$ and $Mg(OH)_2$ should be

82    formed first by reactions described in Eq. 1 and Eq. 2. Two common phases of magnesium

83    oxychloride are typically reported to exist, containing either 3 or 5 $Mg(OH)_2$ molecules, so called

84    the 3-form and 5-form, respectively (Eq. 3) [7,16–18]. The addition of small quantities of

85    hydraulic aluminate minerals (such as CA, $C_3A$, and $C_4AF$) can convert the 5-form magnesium

86    oxychloride to 3-form magnesium oxychloride ($3Mg(OH)_2 \cdot MgCl_2 \cdot 8H_2O$) [18]. It was also

87    reported that the 5-form phase can alter to 3-form over time and that the 3-form is more stable

88    than the 5-form [17]. In concrete exposed to $MgCl_2$, therefore, it is expected that 3-form

89    magnesium oxychloride exists due to the usual presence of $C_3A$ and $C_4AF$. The 3-form

90    magnesium oxychloride is unstable and can dehydrate and lose water at temperatures around

91    65 °C [17].

*(3 or 5)Mg (OH)$_2$ + MgCl$_2$ + 8H$_2$O  →  (3 or 5)Mg(OH)$_2$•MgCl$_2$•8H$_2$O*

*Eq. 3*

*(Secondary Magnesium Oxychloride)*

92

93      The formation of calcium oxychloride can be described as in Eq. 4. Calcium oxychloride

94    was found as platey-shaped crystals in concrete exposed to $MgCl_2$ [1,5,10,19]. The formation of

95    calcium oxychloride has been reported to be very expansive and destructive within the

96    cementitious matrix [1,5]. Calcium oxychloride can form at temperatures above the freezing

97    point of water [1,20] and is unstable at room temperature and lower levels of relative humidity

98    [9,21–23].

*3Ca(OH)$_2$ + CaCl$_2$ + 12H$_2$O  →  3Ca(OH)$_2$•CaCl$_2$•12H$_2$O*

*Eq. 4*

*(Secondary Calcium Oxychloride)*

99

100     MgCl$_2$ deicers can also cause formation of calcium chloroaluminate phases such as

101     Freidel's salt [8,24–27]. A possible reaction for the formation of Freidel's salt in the presence of

102     MgCl$_2$ salt, for example, is shown in Eq. 5 [27]. The formations of magnesium oxychloride,

103     calcium oxychloride, and M-S-H were reported as primary sources for severe deterioration. In

104     contrast, brucite, magnesium sulfate, and Freidel's salt are not generally reported as very

105     destructive components [5,7,8,10,14,28].

$$MgCl_2 + 3CaO \cdot Al_2O_3 \cdot CaSO_4 \cdot 12H_2O \quad \rightarrow \quad 3CaO \cdot Al_2O_3 \cdot CaCl_2 \cdot 10\ H_2O + MgSO_4 \cdot 2H_2O$$

*(Monosulfate)*          *(Freidel's salt)*        *(Magnesium*      *Eq. 5*

*Sulfate Hydrate)*

106

107     In previous studies [1–4,29–31], the influence of NaCl and CaCl$_2$ deicing salts on

108     damage development in cementitious materials has been investigated. It was found that

109     chemical reactions between the matrix and salt solution can result in the formation of additional

110     phases that can cause severe damage in cementitious materials. For NaCl, the source of this

111     chemical phase transition appears to be most likely due to the presence of aluminate phases

112     within the concrete. In the CaCl$_2$ case, the additional phase change was mainly due to the

113     formation of calcium oxychloride, and calcium hydroxide was the main source of this reaction.

114     While the use of NaCl and CaCl$_2$ deicing salts are relatively common practices to remove ice

115     and snow from the surface of roadways and pavement, MgCl$_2$ is also used in some regions. For

116     MgCl$_2$, there have been attempts to investigate the potential physical and chemical changes

117     that may be caused by MgCl$_2$ deicing salts and lead to damage development [5,7,8,10,14,28].

118     However, the interaction between MgCl$_2$ and the cementitious material constituents (i.e., pore

119     solution, calcium hydroxide, aluminate phases, or C-S-H) has not been fully understood.

120     The current research attempts to improve the understanding of the contributions that

121     MgCl$_2$ deicing salt may have in cementitious materials to produce damage. It is hypothesized

122     that the conventional $MgCl_2$–$H_2O$ phase diagram is not fully descriptive of what occurs in

123     cementitious materials when $MgCl_2$ is used. Therefore, it is necessary to develop a phase

124     diagram that is applicable for concrete exposed to $MgCl_2$ deicing salt; this phase diagram can

125     be further used to interpret the damage development in concrete exposed to $MgCl_2$ deicing

126     salts.

127

128     **2.0 Experimental Program**

129     Experiments have been performed on mortar samples and hydrated cement powders (or

130     ground cement paste). These experiments are 1) longitudinal guarded comparative calorimeter

131     (LGCC) equipped with acoustic emission measurement, 2) micro focused X-ray fluorescence

132     (µXRF), 3) low temperature differential scanning calorimetry (LT-DSC), and 4) isothermal micro-

133     calorimetry (IMC). The LGCC experiment was performed to evaluate damage development in

134     mortar samples due to phase changes under thermal cycling. µXRF was performed to evaluate

135     $MgCl_2$ fluid ingress and resultant chloride ion profiles in mortar samples. LT-DSC was performed

136     to detect possible phase transitions and to develop a phase diagram that can be used for

137     cementitious materials exposed to $MgCl_2$ deicing salts. IMC was used to evaluate the rate of

138     reaction that may occur between cementitious materials and $MgCl_2$ deicing salt.

139

140     *2.1     Materials, Mixture Proportioning, Specimen Preparation, and Conditioning*

141     Type I ordinary portland cement (OPC) was used in this study. This cement had a

142     calculated Bogue phase composition of 60 % tricalcium silicate ($C_3S$), 10 % dicalcium silicate

143     ($C_2S$), 9 % tricalcium aluminate ($C_3A$), and 10 % tetracalcium aluminoferrite ($C_4AF$) by mass,

144     and a reported Blaine fineness of 375 $m^2$/kg. The total equivalent alkali was 0.86 % originating

145     from 0.35 % of $Na_2O$ and 0.77 % of $K_2O$, by mass. Aggregates used to prepare mortar

146  specimens consisted of natural sand with a maximum size of 4.75 mm, specific gravity of 2.61,

147  fineness modulus of 2.89, and an absorption value of 2.2 % by mass.

148  To perform LGCC and µXRF experiments, mortar specimens were prepared using a

149  sand volume fraction of 55 % and a water-to-cement ratio (*w/c*) of 0.42 by mass. The mass of

150  cement, water, and sand (in saturated-surface-dry (SSD) condition) were 612 kg, 257 kg, and

151  1435 kg per m$^3$ of total material volume, respectively. The mortar was cast in 25.4 mm × 25.4

152  mm × 300 mm (1 in × 1 in × 11.81 in) molds and the samples were demolded after 24 h. All

153  mortar bars were then sealed in double plastic bags and cured for 28 d in these sealed

154  conditions at 23 °C ± 0.5 °C. After 28 d of curing, the mortar bars were cut using a wet saw to

155  25.4 mm × 25.4 mm × 50.8 mm (1 in × 1 in × 2 in) specimens. These specimens were then

156  placed in a vacuum oven at 65 °C ± 1 °C and a pressure of 20 mm Hg ± 5 mm Hg for 7 d to

157  remove moisture (the ± 1 °C and ± 5 mm Hg are indicative of the nominal operating range

158  encountered when running the experiment). These samples were then vacuum saturated with

159  DI water or $MgCl_2$ solutions before performing experiments.

160  To perform LT-DSC and IMC experiments, powders of hydrated cement paste and

161  calcium hydroxide were used. Cement paste with a water-to-cement ratio (*w/c*) of 0.42 by mass

162  was prepared. The cement paste was cured for one year in a sealed condition. After one year,

163  the cement paste specimens were ground in a mortar and pestle and the 75-µm

164  (No. 200) sieve was used to separate out larger particles. The hydrated cement powder was

165  then stored in a vacuum oven at 65 °C ± 1 °C and a pressure of 20 mm Hg ± 5 mm Hg for 3 d to

166  remove moisture. To perform an LT-DSC experiment, a synthetic pore solution ([K+] = 0.65

167  mol/L, [Na+] = 0.45 mol/L, and [OH-] = 1.10 mol/L) was also prepared in addition to powder

168  samples. This solution concentration was calculated using software for estimation of pore

169  solution properties developed previously (http://concrete.nist.gov/poresolncalc.html) [32] for the

170  cement used in this study (assuming 100 % degree of hydration in a sealed condition).

171

### *2.2 Testing Procedure*

173    As mentioned before, four types of experiments were conducted in this study: 1)
174 longitudinal guarded comparative calorimeter (LGCC) equipped with acoustic emission
175 measurement, 2) micro focused X-ray fluorescence (µXRF), 3) low temperature differential
176 scanning calorimetry (LT-DSC), and 4) isothermal micro-calorimetry (IMC).

177    The LGCC, equipped with acoustic emission measurement, was used to perform the
178 freeze-thaw experiments described in [3,4]. A temperature gradient was generated in the test
179 specimen to produce a one-dimensional heat flow. Two meter bars with known thermal
180 properties were used on the top and bottom of the mortar specimens; and temperatures at
181 different locations were monitored to calculate the heat flow through the specimens. Since
182 acoustic emission (AE) has shown promise in quantifying damage (i.e., cracking) [33], acoustic
183 activity was detected during test by one acoustic sensor attached to the specimen. Wave speed
184 (pulse velocity) was also measured on specimens using a pulsed wave generated by two
185 coupled AE sensors through the length of the specimen before and after the freeze-thaw test to
186 measure the damage index. Samples saturated with 0 %, 0.9 %, 3 %, 5 %, 8 %, 10 %, 13 %,
187 and 15 % (by mass) $MgCl_2$ solutions were used to perform LGCC experiments. The temperature
188 of mortar specimens was varied from 24 °C to -40 °C by using a cold plate. The cooling and
189 heating rates were -2 °C/h and 4 °C/h, respectively. At 24 °C and -40 °C, the temperature was
190 kept constant for 1 h and 4 h, respectively, to allow the specimen to reach thermal equilibrium.
191 The test was complete after one cycle.

192    The µXRF was used to estimate the penetration depth of chloride ions into the
193 specimens through the use of hyperspectral X-ray imaging. After imaging, a full X-ray spectrum
194 for the chloride concentration was obtained over its respective spectral range. This imaging
195 technique is described in [34]. For µXRF experiments, one mortar specimen saturated with DI

196   water (as a reference sample) and one mortar specimen saturated with 20 % (by mass) $MgCl_2$

197   solution were used. They were then broken, exposing a cross section surface of their interior for

198   µXRF imaging.

199         The LT-DSC was used to study possible chemical phase transitions in powder-solution

200   samples. The initial temperature of the test was set to equilibrate at 25 °C. After the initial

201   temperature became stable, the LT-DSC cell was cooled to -90 °C at a cooling rate of -5 °C/min.

202   The specimen temperature was kept constant at this temperature (-90 °C) for one min to allow

203   the specimen to equilibrate. A cycle of heating and cooling was established between -90 °C and

204   70 °C. The specimen was equilibrated again at -90 °C for 5 min; and the temperature of the

205   specimen was increased to 70 °C at a heating rate of 5 °C/min. For the LT-DSC, four different

206   series of experiments were performed: Series I) development of a phase diagram for the $MgCl_2$-

207   $H_2O$ system, Series II) development of a phase diagram for pore solutions and $MgCl_2$, Series III)

208   development of a phase diagram for $Ca(OH)_2$–$MgCl_2$-$H_2O$, and Series IV) development of a

209   phase diagram for a cementitious material exposed to $MgCl_2$ solution (using the hydrated

210   cement powder). For Series I and Series II, a total solution mass of 3 mg to 5 mg was used in

211   LT-DSC. For Series III and Series IV, a 9 mg to 11 mg powder sample was mixed with 9 mg to

212   11 mg of $MgCl_2$ solution and the mixture was tested in the LT-DSC immediately after mixing (0

213   d), 1 d after mixing, and 7 d after mixing.

214         The isothermal micro-calorimeter was used to measure the heat released during the

215   reaction between hydrated cement paste powder or calcium hydroxide powder and $MgCl_2$

216   solution under constant temperature (23 °C ± 0.1 °C). The heat release can be used to

217   determine the rate of reaction. An internal admix ampoule was used to determine the heat of

218   reaction as soon as $MgCl_2$ solution was introduced to and mixed with powder by stirring. For

219   these IMC experiments, 2 g of powder was mixed with 2 g of $MgCl_2$ solution.

220

## 3.0 Results and Discussion

### 3.1 Thermal Response of Mortar samples (LGCC Experiment)

During the LGCC experiment, the thermal response of mortar samples was evaluated. Figure 2 indicates the temperatures at different locations of the specimen and the meter bars. Using the measured temperatures and the thermal properties of the meter bars, the heat flow inward or outward of the mortar samples [3] was calculated and is plotted in Figure 2. During freezing, an increase in the temperature and an exothermic behavior (shown by an arrow in this figure) were observed due to ice formation. During thawing, the specimen temperature remains constant near 0 °C, until the melting of ice concludes, as an endothermic behavior was observed.
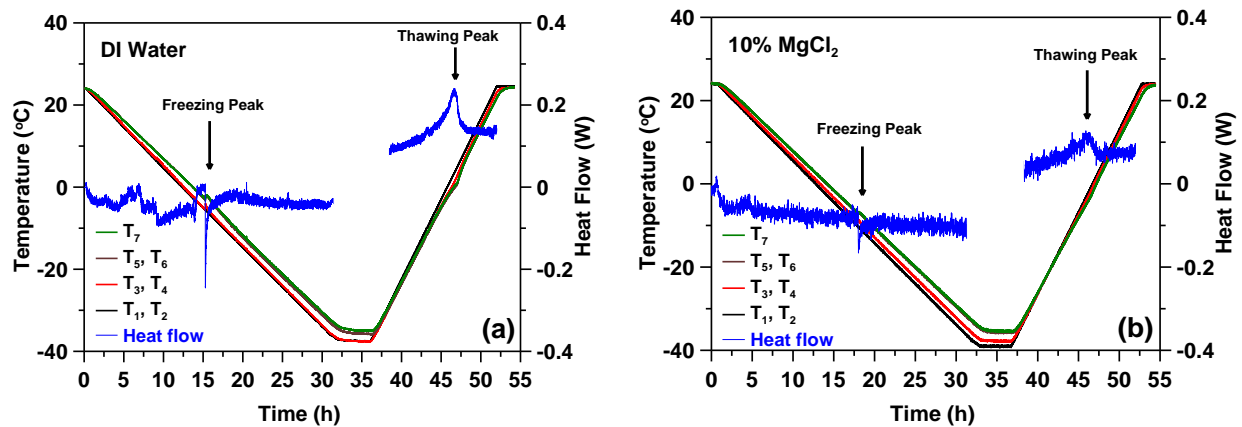


*Figure 2- Temperature at different locations ($T_1$ & $T_2$: temperature between cold plate and bottom meter bar; $T_3$ & $T_4$: temperature between bottom meter bar and specimen; $T_5$ & $T_6$: temperature between specimen and top meter bar; and $T_7$: temperature at the top surface of top meter bar), and heat flow versus time during freeze-thaw cycle for specimens saturated with (a) DI water, and (b) 10 % MgCl$_2$.*

239        The temperatures associated with the exothermic/endothermic behaviors (i.e.,

240    freezing/thawing temperatures) were obtained for all samples and are compared with the

241    conventional $MgCl_2$-$H_2O$ phase diagram in Figure 3. A relatively constant difference between

242    the freezing and thawing temperatures was observed; this is mainly due to supercooling during

243    freezing. A reduction in freezing and thawing temperatures was observed as the solution

244    concentration increases; however, the rate of reduction is less than the one expected from the

245    $MgCl_2$-$H_2O$ (pure) phase diagram (Figure 3). This may be due to $MgCl_2$ being consumed by a

246    replacement of magnesium for calcium in $Ca(OH)_2$ and C-S-H, resulting in the formation of

247    $CaCl_2$, M-S-H, brucite, and magnesium/calcium oxychloride (Eq. 2, Eq. 1, Eq. 3, and Eq. 4);

248    thereby diluting the original solution. For 13 % and 15 % concentrations, the freezing points

249    were even above the liquidus line of conventional $MgCl_2$-$H_2O$. A considerable reduction in fluid

250    ingress into mortar samples during vacuum saturation was observed as the salt concentration

251    increased, which will be discussed in Section 3.3. As a result, the LGCC experiment was not

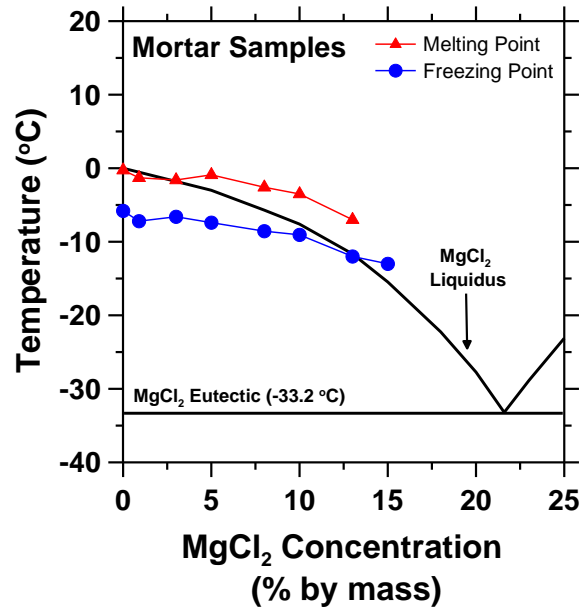252    performed for concentrations of $MgCl_2$ greater than 15 % (by mass).

253

254

*Figure 3 - Freezing and thawing points of solution in mortar samples saturated with $MgCl_2$*

*solutions obtained by LGCC with comparison to the phase diagram of $MgCl_2$ solution (the*

*uncertainty for this measurement was previously measured in [1,3] and the average coefficient*

*of variation was determined to be 9.2 %).*

259

### 3.2 Damage Detection (AE Measurement and LGCC Experiment)

Acoustic emission activity (produced primarily due to cracking) was monitored during the

LGCC experiment to determine freeze-thaw damage. The AE activity (amplitude of events) is

shown in Figure 4 as a function of temperature for specimens saturated by DI water and 10 %

$MgCl_2$ solution, as examples. At the freezing temperature, clusters of AE events develop due to

cracking (~ -5 °C for DI water and ~ -10 °C for 10 % $MgCl_2$). During cooling, the AE activities are

mainly due to hydraulic and osmotic pressures caused by the ice formation. For sample

saturated with 10 % $MgCl_2$, the AE events during cooling spread out after freezing while for

sample saturated with DI water they are more concentrated. This is mainly due to the gradual

additional damage caused by increasing osmotic pressure as the temperature decreases.

270    AE activity is also seen during heating which may be attributed to cracking

271    development/propagation due to stress relaxation and thermal expansion of the specimen

272    during ice melting. The damage on thawing is significantly lower than the damage on freezing.

273    During heating, a cluster of AE events was observed at the moment if ice melting for sample

274    saturated with DI water while no cluster was observed for sample saturated with 10 % $MgCl_2$.

275



276    **(a)**                                    **(b)**
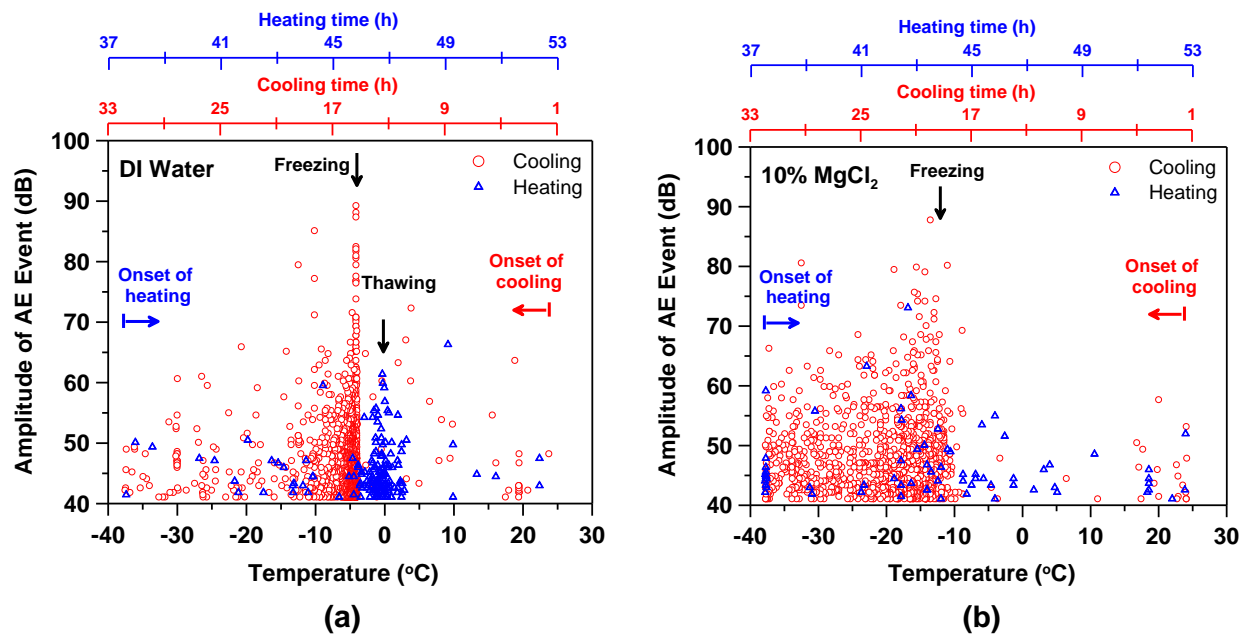
277    *Figure 4 - AE events as a function of temperature during cooling and heating for mortar*

278    *specimens saturated with (a) DI water; and (b) 10 % MgCl₂ solution.*

279

280    A damage index (a measure of the reduction in dynamic elastic modulus) was also

281    determined using the ASTM C597-09 procedure [35] for specimens in two conditions: a)

282    damage caused during immersion time, and b) damage caused during the freeze-thaw cycle.

283    Figure 5a shows the damage index as the $MgCl_2$ concentration increases. Mortar specimens

284    saturated with high concentration $MgCl_2$ solutions (≥10% by mass) indicated damage before the

285    freezing and thawing began, during the time when the samples were immersed in solution. This

13

286 damage appears to correspond to the chemical reactions occurring between $MgCl_2$ and

287 cementitious constituents (Eq. 2, Eq. 1, Eq. 3, and Eq. 4). In contrast, these samples did not

288 show considerable damage due to the freeze-thaw cycle itself. This may be attributed to the fact

289 that a large portion of solution in concrete pores was consumed by the chemical reactions to

290 form magnesium/calcium oxychlorides (solid phases at room temperature, i.e., 23 °C). As a

291 result, further ingress of solution would be prevented due to pore clogging; and thus, the sample

292 would remain unsaturated during the subsequent freeze-thaw cycle.

293 Mortar specimens saturated with low concentration $MgCl_2$ solutions (<10 % by mass)

294 showed a relatively small reduction in dynamic elastic modulus during immersion time, while

295 they showed considerable damage during the subsequent freeze-thaw cycle. For these

296 samples, the hydraulic and osmotic pressures caused by ice formation during freezing and

297 thawing may be the main source of cracking. Figure 5b shows the total cumulative AE signal

298 strength as a function of solution concentration. The samples saturated with 3 % and 5 % $MgCl_2$

299 solution (by mass) showed a relatively higher level of freeze-thaw damage and a greater

300 cumulative AE signal strength. This can be attributed to the critical damage caused by a

301 combination of hydraulic pressure and osmotic pressure during freezing and thawing [36,37].
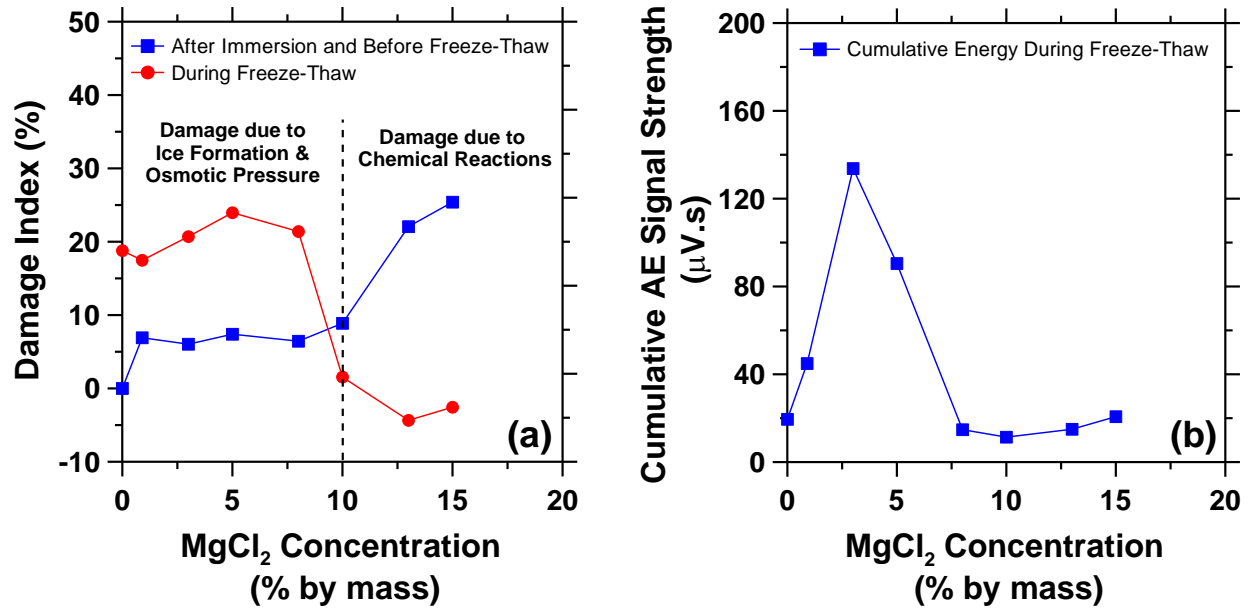
302

303

Figure 5 – (a) Change in the relative dynamic elastic modulus (damage index) due to freeze-
thaw damage for samples saturated with different dosages of MgCl$_2$ solution (the uncertainty
was previously measured in [1,3] and the average coefficient of variations were determined to
be 6.2 % and 15.6 % for damage index and cumulative AE signal strength, respectively).

### 3.3   MgCl$_2$ Fluid Ingress and Chloride Profile (μXRF Experiments)

During vacuum saturation of mortar specimens for the LGCC experiment, a reduction in
fluid absorption into mortar specimens was observed for specimens saturated with high
concentration solutions (≥8 % by mass). As the concentration of solution increased, the amount
of fluid ingress decreased. Therefore, the reduction in degree of saturation (DOS) for mortar
samples tested in the LGCC experiment was determined using Eq. 6  and it is shown in Figure 6
as a function of MgCl$_2$ concentration.

$$Reduction\ in\ DOS = 1 - \frac{V_{abs}}{V_{max}}$$

*Eq. 6*

15

318  where $V_{abs}$ is the volume of the solution absorbed by the samples and $V_{max}$ is the maximum

319  volume of a solution that can be absorbed by the mortar samples used in this study (obtained

320  from the sample saturated with DI water). The reduction in DOS for specimens saturated with

321  MgCl$_2$ solutions with concentrations greater than 8 % (by mass) is most likely attributed to the

322  enhanced formation of brucite, and magnesium/calcium oxychloride that can fill in the pores

323  near the surface of specimens and block the fluid ingress into the mortar samples. In fact,

324  higher volumes of brucite and magnesium/calcium oxychloride should be produced as the

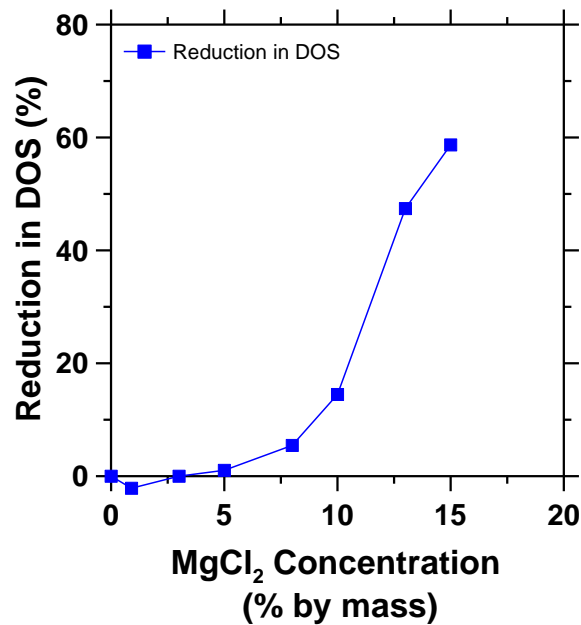325  solution concentration increases.

326



328  *Figure 6 - Reduction in degree of saturation (DOS) for mortar specimens saturated with different*

329  *concentrations of MgCl$_2$ solutions (the uncertainty was measured in* [1,3] *study and the*

330  *maximum standard deviation was determined to be 3 %).*

331

332  To better understand the MgCl$_2$ fluid ingress into mortar samples, two mortar specimens

333  were saturated using only DI water and 20 % MgCl$_2$ solution; and the chloride profile within their

334    depth was determined using µXRF. Figure 7 indicates color-coded image maps for chloride.

335    Yellow and white colors indicate higher concentrations of chlorides, while a black color indicates

336    areas with relatively no chloride. In addition, red color shows areas with relatively lesser

337    intensity of chloride ions than the yellow and white colors. The normalized color intensity within

338    the depth of each sample was also determined using the average value for the middle third of

339    the sample section and is plotted in Figure 7. The core of the specimen is free of chloride while

340    the edges of samples have a higher level of chlorides. This can again provide confirmatory

341    evidence that pores near the specimen surfaces may be blocked by the possible chemical

342    reactions between the cement matrix and $MgCl_2$, thereby preventing further fluid ingress into the

343    sample saturated with the 20 % $MgCl_2$ solution. Aggregates appeared in black color since they

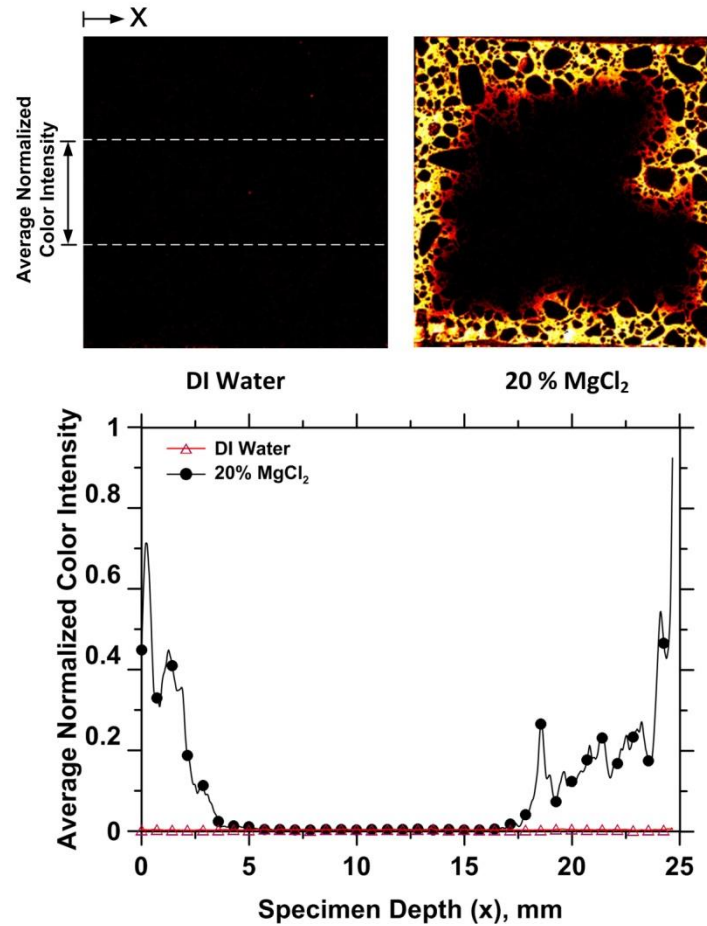344    have quite small porosity and chloride ions cannot penetrate into aggregates.

345



346

Figure 7 - X-ray fluorescence images of mortar samples saturated with DI water and 20 %

MgCl₂ solution and average normalized color intensity within the depth of mortar specimens.

349

### 3.4   Phase Diagram Development (LT-DSC Experiment)

Four series of experiments were performed using powder/solution samples in the LT-DSC to determine the temperature at which phase changes associated with the formation of ice, eutectic solid, calcium oxychloride, and magnesium oxychloride occur. This was done to develop a phase diagram for 1) $MgCl_2$ solution, 2) pore solution and $MgCl_2$, 3) $Ca(OH)_2$ and $MgCl_2$ solution ($Ca(OH)_2$-$MgCl_2$–$H_2O$), and 4) cementitious material (hydrated cement) and $MgCl_2$ solution.

357

358 3.4.1 $MgCl_2$–$H_2O$ solution and Pore Solution Containing $MgCl_2$

359       For the $MgCl_2$–$H_2O$ solution, two endothermic peaks were observed corresponding to

360 eutectic solid and ice melting as the temperature of the sample increased. The eutectic and

361 liquidus peaks for $MgCl_2$ solution are shown in Figure 8a as a function of salt concentration. The

362 experimental results followed the conventional $MgCl_2$-$H_2O$ phase diagram.

363       For the pore solution and $MgCl_2$ system, in addition to the eutectic and ice peaks, two

364 additional endothermic peaks were detected during the sample heating as shown in Figure 8b.

365 For pore solution, the liquidus and eutectic temperatures showed relatively a different behavior

366 than that shown in the $MgCl_2$-$H_2O$ phase diagram. As indicated in Figure 8b, a reduction in the

367 freezing temperature depression was observed for temperatures at which ice forms as the salt

368 concentration increases. In addition, it appears that the eutectic concentration changed to a

369 higher concentration (~ 27 % by mass) than expected from the $MgCl_2$-$H_2O$ phase diagram

370 (21.6 % by mass). Two additional endotherms were observed from phase changes associated

371 with the presence of NaOH and KOH in the pore solution. Endothermic 1 and endothermic 2

372 temperatures most likely reflect the formation of $KCl\cdot H_2O$ (transition temperature at -10.7 °C)

373 and $NaOH\cdot 7H_2O$ (transition temperature at -28.0 °C), respectively [38,39].
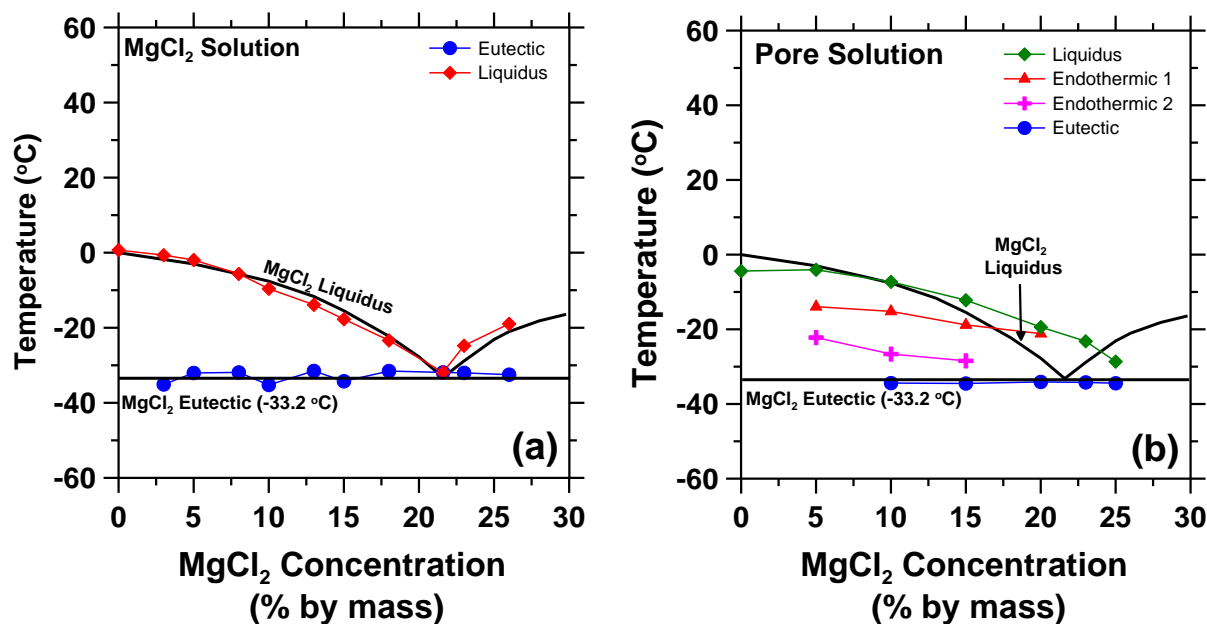
374

*Figure 8 - Comparison of temperatures associated with different phase changes observed in LT-DSC with conventional phase diagram for MgCl₂ solution: a) MgCl₂ solution, b) low alkali pore solution containing MgCl₂ salt (calorimetric reproducibility is reported to be within ± 0.05 % using reference indium metal [40]).*

### 3.4.2   Ca(OH)₂-MgCl₂–H₂O

For Ca(OH)₂ powder with MgCl₂–H₂O solution, two endothermic peaks were observed during the heating of the samples in LT-DSC. The results are shown in Figure 9 and are compared with the phase diagrams for MgCl₂-H₂O, and CaCl₂–H₂O, and the calcium oxychloride formation line. The endotherm that was observed at temperatures greater than 0 °C is most likely due to the formation of calcium oxychloride since its formation temperature follows the calcium oxychloride liquidus line. The endotherm observed at 0 °C is compatible with pure ice melting. It appears MgCl₂ was consumed through a very rapid chemical reaction between MgCl₂ and Ca(OH)₂ to form Mg(OH)₂ (brucite) and CaCl₂ (Eq. 2); the produced CaCl₂ reacted with the remaining Ca(OH)₂ and calcium oxychloride was formed.

391    Mg(OH)$_2$ is a relatively stable material and does not decompose until the temperature

392    reaches approximately 400 °C. There is a possibility that magnesium oxychloride was also

393    formed and it can decompose (lose some of its water) during the temperature range applied in

394    this study. However, no endotherm was observed associated with magnesium oxychloride

395    decomposition. This may be due to the fact that the reaction between MgCl$_2$ and Ca(OH)$_2$ to

396    form Mg(OH)$_2$ (brucite) and CaCl$_2$ was very fast (Section 3.5) and no MgCl$_2$ remained to form

397    magnesium oxychloride. It should be noted that mixing calcium hydroxide powder with MgCl$_2$

398    solution with a concentration greater than 15 % could not be achieved, due to a very fast

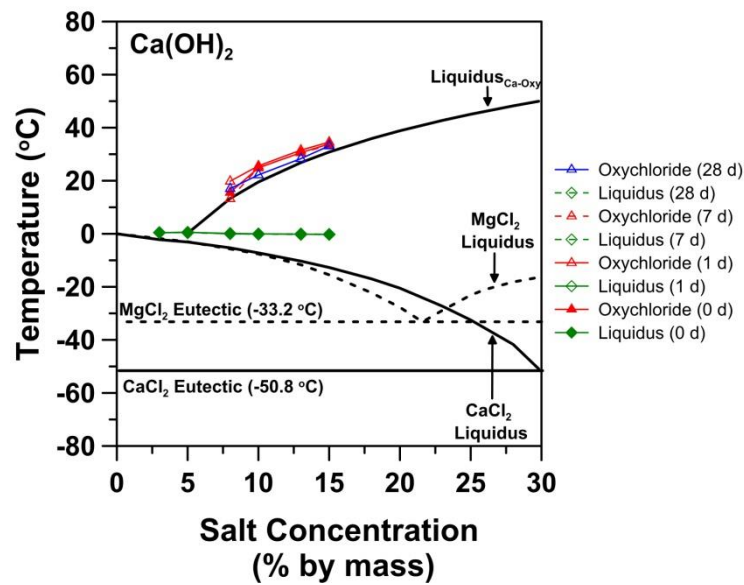399    reaction and near immediate solidification.

400



401

402    *Figure 9 - Phase diagram for a system containing MgCl$_2$, Ca(OH)$_2$, and H$_2$O (the liquidus line for*

403    *the formation of calcium oxychloride was obtained from [1] as shown liquidus$_{Ca-Oxy}$; CaCl$_2$-H$_2$O*

404    *phase diagram and liquidus$_{ca-oxy}$ are plotted as a function of CaCl$_2$ concentration while MgCl$_2$-*

405    *H$_2$O phase diagram is plotted as a function of MgCl$_2$ concentration).*

406

407    3.4.3    Cementitious Material Exposed to $MgCl_2$ solution

408          Hydrated cement powder (ground paste) and $MgCl_2$ solution behaved quite differently

409    than the conventional $MgCl_2$–$H_2O$ phase diagram. Three endothermic peaks were observed

410    during the heating of the samples in LT-DSC. The results are shown in Figure 10 and are

411    compared with the phase diagrams for $MgCl_2$-$H_2O$, and $CaCl_2$–$H_2O$, and the calcium oxychloride

412    formation line. As expected, hydrated cement powder and $MgCl_2$ solution did not follow the

413    conventional $MgCl_2$-$H_2O$ phase diagram. Instead, the detected eutectic and liquidus lines

414    matched quite well with what would be expected from the $CaCl_2$-$H_2O$ phase diagram [1].

415          An additional endothermic behavior that was observed at temperatures greater than 0 °C

416    is most likely due to the dehydration of magnesium oxychloride, since its temperature does not

417    completely follow the liquidus line for the formation of calcium oxychloride. However, for lower

418    concentrations (≤15 % by mass), it seems that magnesium oxychloride is not stable and can

419    convert to calcium oxychloride at later ages (7 d, Figure 10b) since the temperature at which

420    oxychloride was detected moved to a lower temperature (i.e., liquidus line associated with

421    calcium oxychloride formation) as the exposure time increased.

422          For higher concentrations (> 15 % by mass), the additional endothermic peak was not

423    observed immediately after mixing the hydrated cement powder and $MgCl_2$ solution (Figure

424    10a); it was only detected after 7 d (Figure 10b). For concentrations greater than 15 % by mass,

425    the quick formation of brucite may consume whole calcium hydroxide and prevent the formation

426    of calcium oxychloride. At later ages (7 d), brucite can react with remained $MgCl_2$ in the solution

427    and form magnesium oxychloride. At lower concentrations (< 15 % by mass), however, the

428    amount of $MgCl_2$ in the solution may not be sufficient to consume whole calcium hydroxide for

429    brucite formation. Therefore, remained calcium hydroxide may react with produced $CaCl_2$ to

430    form calcium oxychloride. At lower concentrations, the conversion between calcium oxychloride

431  and magnesium oxychloride at later ages may show that magnesium oxychloride may be a

432  more stable material than calcium oxychloride.

433      A logarithmic trend line was fitted to the data points associated with the dehydration of

434  magnesium oxychloride (i.e., when magnesium oxychloride loses some water) and is presented

435  in Eq. 7 and shown as the Mg-Oxy line in Figure 10.

$$T = 25.32 \ln \frac{C_o}{C^*} \qquad\qquad R^2 = 0.97 \qquad\qquad Eq.\ 7$$

436

437  where T (°C) is the temperature at which magnesium oxychloride begins to dehydrate, $C_o$ (% by

438  mass) is the initial concentration of $MgCl_2$ solution, and $C^*$ (= 2.58 %) is the theoretical minimum

439  concentration of $MgCl_2$ solution at which the magnesium oxychloride begins to dehydrate (as

440  $3Mg(OH)_2 \cdot MgCl_2 \cdot 8H_2O$ loses some of its water (see Section 1.0)).
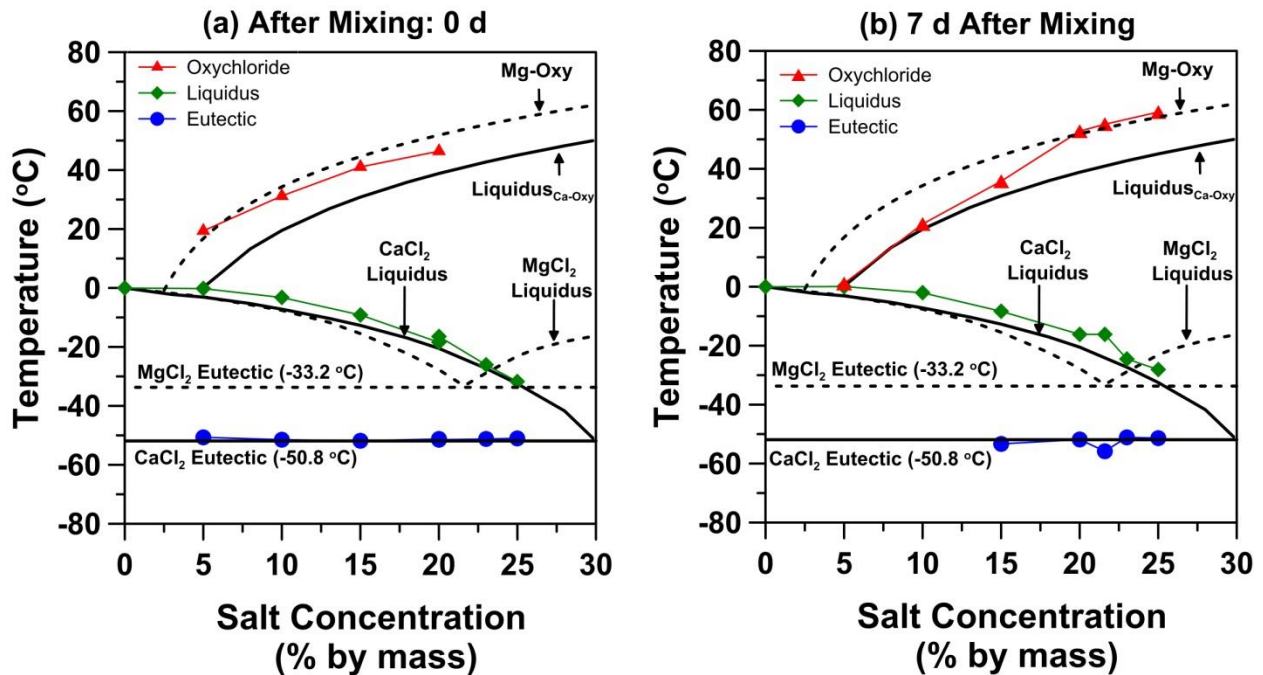
441



443  *Figure 10 - Comparison of temperatures associated with different phase changes for hydrated*

444  *cement powder and $MgCl_2$ solution in LT-DSC with phase diagrams for $MgCl_2$-$H_2O$, $CaCl_2$-$H_2O$,*

445     *calcium oxychloride (shown by liquidus$_{Ca-Oxy}$), and magnesium oxychloride (shown by Mg-Oxy)*

446     *at different exposure ages: a) immediately after mixing the solution and powder, and b) 7 days*

447     *after mixing the solution and powder.*

448

449     **3.5   Reaction Rate between Powder and MgCl$_2$ Solution (IMC Experiment)**

450     To assess the rate of reaction between hydrated cement paste or calcium hydroxide and

451     MgCl$_2$ solutions, isothermal calorimetry experiments were performed. The heat flow was

452     measured as soon as MgCl$_2$ solution was mixed with dry powder (hydrated cement paste or

453     Ca(OH)$_2$) and it is shown in Figure 11. Blending the Ca(OH)$_2$ powder with DI water showed a

454     very small amount of heat release. This may be attributed mainly to the heat release caused by

455     internal mixing and the heat of wetting. A considerably higher heat release was observed during

456     blending hydrated cement powder and DI water that is most likely associated with internal

457     mixing, heat of wetting, and the heat of hydration of any unreacted cement (or unreacted C$_3$A).

458     As the concentration of the solution increased, the heat release increased for both

459     Ca(OH)$_2$ and hydrated cement powders. The majority of the heat release occurred within the

460     first 10 min, illustrating the high rate of reaction between Ca(OH)$_2$ or the hydrated cement

461     powder and MgCl$_2$ solutions to form brucite and/or calcium/magnesium oxychloride. As the salt

462     concentration increases, the increase in the heat release appears to be higher for the hydrated

463     cement powder than for pure calcium hydroxide (assuming 25 % calcium hydroxide in the

464     hydrated cement powder). This additional heat release for the hydrated cement powder may be

465     due to the reaction between aluminate phases in the hydrated cement powder and MgCl$_2$ to

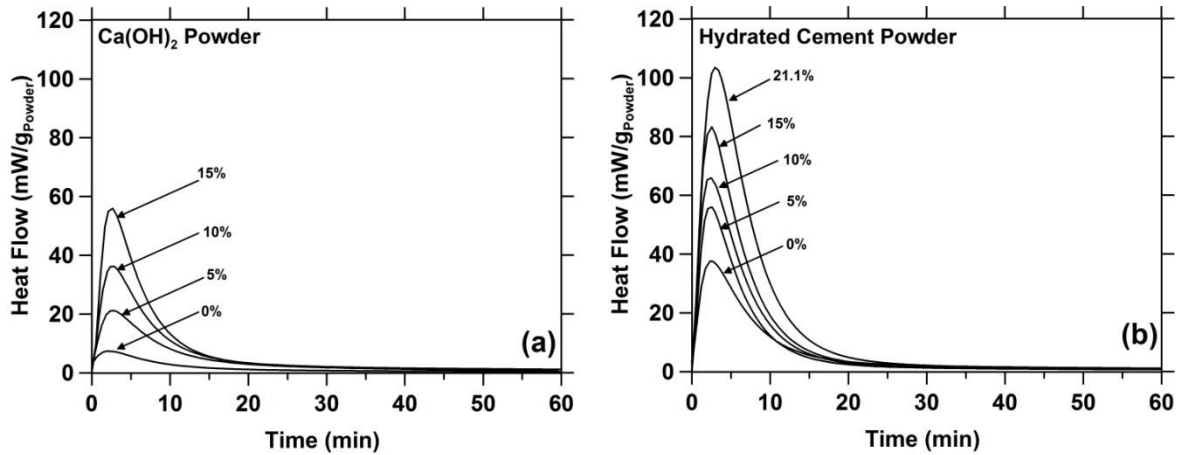466     form magnesium sulfate hydrate and Freidel's salt (Eq. 5).

467

469   *Figure 11 - Heat flow curves (normalized by the amount of powder) measured at 23 °C as a*

470   *function of time for a) Ca(OH)$_2$ powder and MgCl$_2$ solution, and b) hydrated cement powder and*

471   *MgCl$_2$ solution. (Percentages indicate MgCl$_2$ solution concentration by mass, the precision is*

472   *reported within ± 20 µW [41]).*

473

## 474   4.0 Conclusions

475   This paper shows that the chemical reactions between MgCl$_2$ and cementitious

476   constituents can result in the formation of additional chemical phases such as CaCl$_2$, brucite,

477   magnesium oxychloride, and calcium oxychloride in concrete. The additional chemical phases

478   can result in damage in concrete, as well as changes in the behavior of the remaining solution in

479   concrete under thermal variations.

480   Thermal evaluation of cementitious samples showed that the MgCl$_2$-H$_2$O solution in

481   concrete does not behave as expected from the pure MgCl$_2$-H$_2$O phase diagram. This is mainly

482   due to the chemical reactions between MgCl$_2$ and concrete constituents and the formation of

483   additional chemical phases. A phase diagram was proposed for a cementitious material

484   exposed to MgCl$_2$. It was observed that it is relatively similar to the pure CaCl$_2$-H$_2$O phase

485   diagram, with additional phase changes associated with the formation of magnesium

486   oxychloride and calcium oxychloride phases.

487    Damage of mortar samples was also evaluated when they were exposed to thermal

488    cycling and $MgCl_2$ solutions. The damage observed in mortar samples saturated with low

489    concentration $MgCl_2$ solution (<10% by mass) was mainly due to hydraulic pressure and

490    osmotic pressure caused by ice formation. Exposure to high concentration $MgCl_2$ solutions (≥10

491    % by mass) showed damage (reduction in dynamic elastic modulus) prior to any thermal cycling

492    (before freeze-thaw testing, when the samples were immersed in the solution). This may be due

493    to the formation of magnesium oxychloride or/and calcium oxychloride at room temperature (23

494    °C). The further change in dynamic elastic modulus after one freeze-thaw cycle was not

495    considerable for specimens saturated with high concentration $MgCl_2$ solutions (≥10 % by mass).

496    This may be due to the fact that a large portion of solution in concrete pores was consumed by

497    the formations of calcium/magnesium oxychloride and brucite, and the sample remained

498    unsaturated. The formation of M-S-H may also be another source of damage or change in fluid

499    ingress into mortar samples. However, more research is needed to understand the influence of

500    M-S-H formation on damage development and fluid ingress in cementitious materials exposed

501    to $MgCl_2$ solutions.

502

503    **5.0 Acknowledgment**

511   Highway Administration and the Indiana Department of Transportation, nor do the contents

512   constitute a standard, specification, or regulation.

513

514   **6.0 References**

515   [1]   Y. Farnam, S. Dick, A. Wiese, J. Davis, D. Bentz, J. Weiss, The Influence of Calcium
516         Chloride Deicing Salt on Phase Changes and Damage Development in Cementitious
517         Materials, Submitt. to Cem. Concr. Compos. (2014) 1–41.

518   [2]   Y. Qian, Y. Farnam, J. Weiss, Using Acoustic Emission to Quantify Freeze–Thaw
519         Damage of Mortar Saturated with NaCl Solutions, in: Proc. 4th Int. Conf. Durab. Concr.
520         Struct., Purdue University Libraries Scholarly Publishing Services, 2014: pp. 32–37.
521         doi:10.5703/1288284315379.

522   [3]   Y. Farnam, D. Bentz, A. Sakulich, D. Flynn, J. Weiss, Measuring Freeze and Thaw
523         Damage in Mortars Containing Deicing Salt Using a Low-Temperature Longitudinal
524         Guarded Comparative Calorimeter and Acoustic Emission, Adv. Civ. Eng. Mater. 3 (2014)
525         316–337. doi:10.1520/ACEM20130095.

526   [4]   Y. Farnam, D. Bentz, A. Hampton, J. Weiss, Acoustic emission and low temperature
527         calorimetry study of freeze and thaw behavior in cementitious materials exposed to NaCl
528         salt (In Press), Transp. Res. Board Rec. (2014) 1–18.

529   [5]   L. Sutter, K. Peterson, S. Touton, T. Van Dam, D. Johnston, Petrographic evidence of
530         calcium oxychloride formation in mortars exposed to magnesium chloride solution, Cem.
531         Concr. Res. 36 (2006) 1533–1541. doi:10.1016/j.cemconres.2006.05.022.

532   [6]   X. Shi, L. Fay, M.M. Peterson, Z. Yang, Freeze–thaw damage and chemical change of a
533         portland cement concrete in the presence of diluted deicers, Mater. Struct. 43 (2010)
534         933–946. doi:10.1617/s11527-009-9557-0.

535   [7]   G.A. Julio-Betancourt, Effect of De-icers and Anti-icer Chemicals on the Durability,
536         Microstructure, and Properties of Cement-based Materials, University of Toronto, 2009.

537   [8]   L. Sutter, K. Peterson, G. Julio-Betancourt, D. Hooton, T.V. Dam, K. Smith, The
538         deleterious chemical effects of concentrated deicing solutions on Portland cement
539         concrete, Final Report for the South Dakota Department of Transportation, 2008.

540   [9]   M. Collepardi, L. Coppola, C. Pistolesi, Durability of concrete structures exposed to
541         CaCl2 based deicing salts, in: V.M. Malhotra (Ed.), Durab. Concr. ACI SP-145, 3rd
542         CANMET/ACI Int. Conf., 1994: pp. 107–120.

543   [10]  K. Peterson, G. Julio-Betancourt, L. Sutter, R.D. Hooton, D. Johnston, Observations of
544         chloride ingress and calcium oxychloride formation in laboratory concrete and mortar at
545         5°C, Cem. Concr. Res. 45 (2013) 79–90. doi:10.1016/j.cemconres.2013.01.001.

546    [11]   D. Bonen, Composition and Appearance of Magnesium Silicate Hydrate and Its Relation
547           to Deterioration of Cement-Based Materials, J. Am. Ceram. Soc. 75 (1992) 2904–2906.
548           doi:10.1111/j.1151-2916.1992.tb05530.x.

549    [12]   H. Lee, obert D. Cody, A.M. Cody, P.G. Spry, Observations on brucite formation and the
550           role of brucite in Iowa highway concrete deterioration, Environ. Eng. Geosci. 8 (2002)
551           137–145.

552    [13]   H. Lee, R.D. Cody, A.M. Cody, P.G. Spry, Effects of various deicing chemicals on
553           pavement concrete deterioration, in: Mid-Continent Transp. Symp. 2000 Proc., 2000: pp.
554           151–155.

555    [14]   M. Santhanam, M. Cohen, J. Olek, Study of Magnesium Ion Attack in Portland Cement
556           Mortars, in: G. Grieve, G. Owens (Eds.), Proc. 11th Int. Congr. Chem. Cem., Durban,
557           South Africa, 2003: pp. 1460–1474.

558    [15]   D. Bonen, M.D. Cohen, Magnesium sulfate attack on portland cement paste-I.
559           Microstructural analysis, Cem. Concr. Res. 22 (1992) 169–180. doi:10.1016/0008-
560           8846(92)90147-N.

561    [16]   T. Demediuk, W. Cole, H. Hueber, Studies on magnesium and calcium oxychlorides,
562           Aust. J. Chem. 8 (1955) 215. doi:10.1071/CH9550215.

563    [17]   W. Cole, T. Demediuk, X-Ray, thermal, and Dehydration studies on Magnesium
564           oxychlorides, Aust. J. Chem. 8 (1955) 234. doi:10.1071/CH9550234.

565    [18]   D. Dehua, Z. Chuanmei, The effect of aluminate minerals on the phases in magnesium
566           oxychloride cement, Cem. Concr. Res. 26 (1996) 1203–1211. doi:10.1016/0008-
567           8846(96)00101-9.

568    [19]   Y. Farnam, T. Washington, W.J. Weiss, The effect of $CaCl_2$ deicing salt and degree of
569           saturation on transport properties of mortar, 2014.

570    [20]   I.I. Vol'nov, E.I. Latysheva, Separation of calcium chloride from Solvay spent liquor
571           through calcium hydroxichloride, J. Appl. Chem. U.S.S.R. 30 (1957) 1039–1046.

572    [21]   C. Shi, Formation and stability of $3CaO \cdot CaCl_2 \cdot 12H_2O$, Cem. Concr. Res. 31 (2001)
573           1373–1375. doi:10.1016/S0008-8846(01)00576-2.

574    [22]   S. Chatterji, Mechanism of the $CaCl_2$ attack on portland cement concrete, Cem. Concr.
575           Res. 8 (1978) 461–467. doi:10.1016/0008-8846(78)90026-1.

576    [23]   L. Berntsson, S. Chandra, Damage of concrete sleepers by calcium chloride, Cem.
577           Concr. Res. 12 (1982) 87–92. doi:10.1016/0008-8846(82)90102-8.

578    [24]   A. Mesbah, M. François, C. Cau-dit-Coumes, F. Frizon, Y. Filinchuk, F. Leroux, et al.,
579           Crystal structure of Kuzel's salt $3CaO \cdot Al_2O_3 \cdot 1/2CaSO_4 \cdot 1/2CaCl_2 \cdot 11H_2O$ determined by

580       synchrotron powder diffraction, Cem. Concr. Res. 41 (2011) 504–509.
581       doi:10.1016/j.cemconres.2011.01.015.

582   [25]  P. Brown, J. Bothe, The system CaO-Al2O3-CaCl2-H2O at 23±2 °C and the mechanisms
583       of chloride binding in concrete, Cem. Concr. Res. 34 (2004) 1549–1553.
584       doi:10.1016/j.cemconres.2004.03.011.

585   [26]  Y. Bu, D. Luo, J. Weiss, Comparing Fick's Second Law and the Nernst-Planck Approach
586       in the Prediction of Chloride Ingress in Concrete Materials, Under Rev. (2014).

587   [27]  A.K. Suryavanshi, J.D. Scantlebury, S.B. Lyon, Mechanism of Friedel's salt formation in
588       cements rich in tri-calcium aluminate, Cem. Concr. Res. 26 (1996) 717–727.
589       doi:10.1016/S0008-8846(96)85009-5.

590   [28]  X. Shi, Y. Liu, M. Mooney, B. Hubbard, L. Fay, A. Leonard, Effect of Chloride-based
591       Deicers on Reinforced Concrete Structures, 2010.

592   [29]  W. Jones, Y. Farnam, P. Imbrock, J. Sprio, C. Villani, J. Olek, et al., An Overview of Joint
593       Deterioration in Concrete Pavement: Mechanisms, Solution Properties, and Sealers,
594       2013. doi:10.5703/1288284315339.

595   [30]  W. Li, M. Pour-Ghaz, J. Castro, J. Weiss, Water absorption and critical degree of
596       saturation relating to freeze-thaw damage in concrete pavement joints, J. Mater. Civ.
597       Eng. 24 (2012) 299–307. doi:10.1061/(ASCE)MT.1943-5533.0000383.

598   [31]  C. Villani, Y. Farnam, T. Washington, J. Jain, J. Weiss, Performance of Conventional
599       Portland Cement and Calcium Silicate Based Carbonated Cementitious Systems During
600       Freezing and Thawing in the presence of Calcium Chloride Deicing Salts (In Press),
601       Transp. Res. Board. (2014).

602   [32]  D.P. Bentz, A virtual rapid chloride permeability test, Cem. Concr. Compos. 29 (2007)
603       723–731. doi:10.1016/j.cemconcomp.2007.06.006.

604   [33]  Y. Farnam, M. Geiker, D. Bentz, J. Weiss, Using Acoustic Emission Waveform
605       Characterization to Ascertain Where Cracks Originate in Concrete (Submitted), Cem.
606       Concr. Compos. (2014).

607   [34]  J.M. Davis, D.E. Newbury, P. rao Rangaraju, S. Soundrapanian, C. Giebson, Milli X-ray
608       fluorescence X-ray spectrum imaging for measuring potassium ion intrusion into concrete
609       samples, Cem. Concr. Compos. 31 (2009) 171–175.
610       doi:10.1016/j.cemconcomp.2008.12.005.

611   [35]  ASTM, ASTM C597- Standard test method for pulse velocity through concrete, in: ASTM
612       International, West Conshohocken, PA, 2009.

613   [36]  T. Powers, A working hypothesis for further studies of frost resistance of concrete, in: J.
614       Am. Concr. Inst., Portland Cement Association, Detroit, Michigan, 1945: pp. 245–272.

615  http://www.concrete.org/PUBS/JOURNALS/OLJDetails.asp?Home=JP&ID=8684
616  (accessed March 15, 2013).

617  [37]  T.C. Powers, The physical structure and engineering properties of concrete, Res. Dep.
618  Bull. Portl. Cem. Assoc. 90 (1958) 27 pages.

619  [38]  W. van der Tempel, Eutectic Freeze Crystallization: Separation of Salt and Ice, Delf
620  University of Technology, 2012.

621  [39]  F.F. Purdon, V.W. Slater, Aqueous Solution and The Phase Diagram, First Edit, Butler &
622  Tanner Ltd., Frome and London, London, Great Britain, 1946.

623  [40]  T. Instrument, Q2000 Differential Scanning Calorimeter Brochure,
624  Http://www.tainstruments.com/. (2012) 30.

625  [41]  T. Instrument, TAM AIR Isothermal Calorimetry, Http://www.tainstruments.com/. (2013)
626  20.

627